ACS OMEGA

Article

Cite This: ACS Omega 2019, 4, 39−47

http://pubs.acs.org/journal/acsodf

Randomization and Constraint of Molecular Alignment and Orientation: Temperature-Dependent Anisotropy and Phase Transition in Vapor-Deposited Thin Films of an Organic Cross-Shaped Molecule

Masahito Oh-e,*,† Hidenori Ogata,† and Fumito Araoka‡

†Institute of Photonics Technologies, Department of Electrical Engineering, National Tsing Hua University, 101 Sec. 2 Kuang-Fu Road, Hsinchu 30013, Taiwan

‡RIKEN Center for Emergent Matter Science, 2-1 Hirosawa, Wako, Saitama 351-0198, Japan

Supporting Information

ABSTRACT: We observe potential randomization and constraint of molecular alignment and orientation in an organic semiconductor molecule with increasing temperature up to the phase-transition temperature. Variable-angle spectroscopic ellipsometry and second-harmonic generation are used to study the changes in the molecular alignment in vapor-deposited organic thin films as samples are heated and cooled in a cycle from room temperature to the phase-transition temperature. The films consist of sterically bulky and cross-shaped molecules, 2-cyano-9,10-di(2-naphthyl)anthracene, and the anisotropy of its two moieties is probed. Anisotropic molecular alignment with respect to the surface normal in as-deposited amorphous films changes with the film thickness, which increases slightly with increasing substrate temperature. Moreover, the axis near the long axis of the anthracene moiety changes significantly with respect to the surface normal from the magic angle to isotropic alignment, showing monotonically decreasing anisotropy. Interestingly, the anisotropy of the axis near the long axis of the anthracene moiety disappears before the phase-transition temperature. In contrast, the axis near the short axis of the anthracene moiety exhibits a notable characteristic change in the temperature-dependent alignment during the heating process; although the anisotropy initially decreases, it significantly increases as the temperature approaches the phase transition. At a certain temperature during heating, the film thickness shows a discontinuous jump, similar to a first phase transition, while the anisotropic molecular alignment completely disappears. During the cooling process after the phase transition, however, the properties of the films are irreversibly changed, and anisotropic molecular alignment is no longer observed; thus, the samples become completely isotropic.

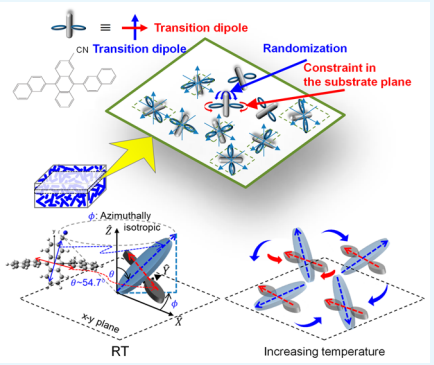

INTRODUCTION

Molecular alignment and orientation are attracting considerable attention in the field of organic semiconductor materials (OSCs),[1−10] which are employed in organic light-emitting diodes (OLEDs),[11] organic photovoltaics,[12] and organic thin-film transistors.[13] Unlike molecular orientation, molecular alignment specifies the distribution of molecular axes that have mirror symmetry with respect to a plane perpendicular to an anisotropic axis of molecular arrangement. Anisotropic alignment and orientation of organic molecules often play a vital role in determining the properties of thin films and hence electronic device characteristics, such as driving voltage and carrier transport properties. In particular, the molecular alignment should be controlled for OLEDs to improve their device characteristics: for example, certain molecular alignments can enhance the light out-coupling efficiency,[14,15] device lifetime,[16] charge mobility,[17−19] energy transfer,[20] and so on. However, even if the molecular alignment in device layers is potentially controlled, the extent to which molecular alignment can be tuned in amorphous states made from a particular compound, as well as the physical and mechanistic origins of this effect, must be understood.

Although anisotropy with respect to the surface normal in OSC thin films is not surprising from the viewpoint of surface science,[21] the recently raised issues on anisotropy in amorphous films are significant,[1−3,6,10] leading to active studies on molecular alignment in the organic amorphous thin films used in OLEDs. Generally, an anisotropic molecular shape is correlated with molecular alignment, and large anisotropy in the molecular shape gives rise to large alignment anisotropy in amorphous films, and hence, large optical anisotropy.[2−4,17] Presumably, this is due to molecular interactions with surfaces and other nearby molecules through dipole and van der Waals interactions, excluded volume effects, etc. Dopant molecules

Received: September 28, 2018
Accepted: December 14, 2018
Published: January 2, 2019

DOI: 10.1021/acsomega.8b02560
ACS Omega 2019, 4, 39−47

are also influenced by the molecular alignment of their host molecules, leading to the alignment of dopant molecules in the host films.[22−25] As the Marcus theory[26] shows, the charge transport rate between molecules is highly dependent on the overlap and coupling of orbitals between molecules; therefore, molecular alignment in charge transport layers influences charge transport rates and in turn the device characteristics.[27,28] Molecular alignment is variable depending on the substrate temperature during vapor deposition.[4]

During vapor-deposition processes, however, the surface mobility of molecules is an important factor determining molecular alignment, orientation, and packing structures on substrates, competing with the thermodynamic force.[29−34] The deposition rate and temperature during vapor deposition govern the surface mobility of molecules;[34] if the deposition is too fast, molecules cannot reach equilibrium at surfaces, and if the temperature is too low, the rearrangement of surface molecules is too slow to equilibrate. With this mechanistic origin, thermodynamically and kinetically stable organic amorphous states have been created.[29] Subsequently, continuously tunable and thermally stable molecular orientation of OSC materials has been reported with a parametric ratio between the substrate temperature and glass transition temperature T_g.[34] Indeed, attaining thermally and kinetically stable packing of molecules in deposited films by controlling the temperature and deposition rate has been well studied. However, simple temperature scanning of as-deposited substrates has not been carefully reported to reveal the molecular alignment in OSC thin films by heating and cooling in the cycle from room temperature (RT) to the phase-transition temperature. In particular, this is the case with bulky molecules with a unique cross shape, in which the anisotropy of two moieties in the molecule can be simultaneously probed.

On the other hand, we have demonstrated how nonlinear optical spectroscopy is powerful enough to probe the molecular alignment and orientation of OSC materials for OLEDs.[21] Although ellipsometry is a viable tool for analyzing molecular alignment,[1,35,36] it cannot distinguish the magic angle and isotropic alignment, whereas second-order nonlinear probing techniques[37] can clarify these different molecular alignments, as we have successfully demonstrated. We have also reported the molecular alignment of a uniquely bulky, cross-shaped molecule, clearly observing its anisotropy by quantitatively analyzing how molecules sit in as-deposited thin films on average using an advanced technique beyond linear optics, called sum-frequency vibrational spectroscopy.[21]

In this paper, a simple heating and cooling cycle is applied to as-deposited OSC films to observe how the molecular alignment of sterically bulky, cross-shaped molecules with a small shape anisotropy changes during the cycle from RT to the phase-transition temperature. In particular, we can independently probe two different moieties of the molecule in terms of molecular alignment because the molecule has two distinctive directional transition dipole moments in the applied spectral range. We use not only spectroscopic ellipsometry but also second-harmonic generation (SHG) to more carefully probe changes in molecular alignment; therefore, the magic angle anisotropic alignment is clearly distinguishable with isotropy.

METHODS

As a uniquely shaped molecule, 2-cyano-9,10-di(2-naphthyl)-anthracene (CADN) is used in this study, and its chemical structure is shown in Figure 1; the anthracene and two naphthalene moieties, which are not in the same plane, make a cross shape. CADN shows two main absorption bands at ∼250 and ∼420 nm, assigned to the transition dipole moments near the long (y) and short (x) axes of the anthracene moiety, respectively, as per density functional theory (DFT) calculations. The molecular structure of CADN is optimized at the B3LYP/6-31G level using Gaussian 09,[38] and a single-point time-dependent DFT calculation is then performed at the B3LYP/6-31G(d) level. The calculated energy and dipole moments for the transitions from the ground state to the excited states are summarized in Supporting Information. Based on the calculated wavelength and oscillator strength, the absorption bands at ∼250 and ∼420 nm can be assigned to the transitions from the ground state to the excited states at 252.51 and 419.94 nm, with oscillator strengths of 0.7865 and 0.1863, respectively (Table S1). The corresponding transition dipole moment to the absorption band at ∼250 nm is $x = -0.662$, $y = -2.4574$, $z = -0.2476$, and that at ∼420 nm is $x = 1.5461$, $y = -0.4293$, $z = -0.0234$ (Table S1). These two transition dipole moments are almost orthogonal, while the transition dipole moment at ∼250 nm, which is due to the CN atomic group attached to the anthracene moiety, is slightly tilted by ∼16° from the y-axis. These assignments are very similar to those reported for the 2-methyl-9,10-di(2-naphthyl)anthracene (MADN) molecule.[21]

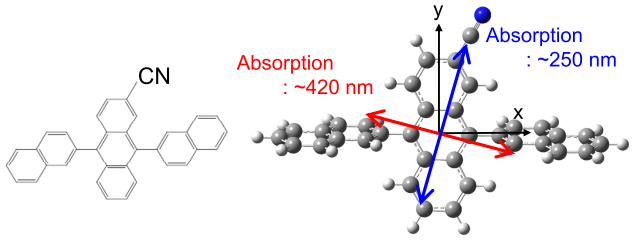

Figure 1. Chemical structure of CADN and the directions of the two transition dipole moments in the molecule.

N,*N*′-Di(1-naphthyl)-*N*,*N*′-diphenyl-(1,1′-biphenyl)-4,4′-diamine) (NPB) is also prepared as a reference, which has been more thoroughly studied by other groups.[2,6,10,15,34,39,40] The sample films are formed by vacuum vapor deposition on Si wafer substrates. Each substrate is cleaned with a 1.0% tetramethylammonium hydroxide aqueous solution and subsequently rinsed with pure water (>18 Ω cm). After being dried with N_2 gas, the surface of the substrates is cleaned by UV−ozone generation. Then, samples are thermally vapor-deposited onto the substrates at RT in a vacuum chamber of less than 10^{-4} Pa at the evaporation rate of ∼0.1 nm/s. The thickness of the films is set to 100 nm. The films are not thermally treated until the measurements.

Variable-angle spectroscopic ellipsometry (VASE)[35,36] is performed using a fast spectroscopic ellipsometer (M-2000U, J. A. Woollam Co., Inc.). Measurements are recorded at multiple incidence angles ranging from 45 to 75° with 5° steps, and experimental ellipsometric parameters Ψ and Δ are simultaneously obtained throughout the spectral region from 245 to 1000 nm. The samples are heated and cooled in a cycle between 25 and 145 °C (CADN) or 115 °C (NPB) in 5 °C intervals. At each temperature, measurements are recorded after stabilizing for 1 min. Using an iterative procedure, namely, the least-squares minimization, unknown optical

DOI: 10.1021/acsomega.8b02560
ACS Omega 2019, 4, 39−47

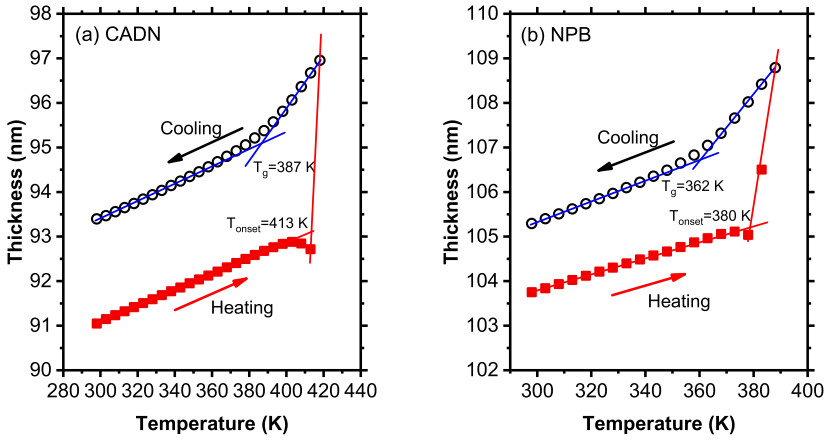

Figure 2. Dependence of the film thickness on temperature during a single heating and cooling cycle from RT to phase transition: (a) CADN; (b) NPB. The thickness data are obtained by VASE.

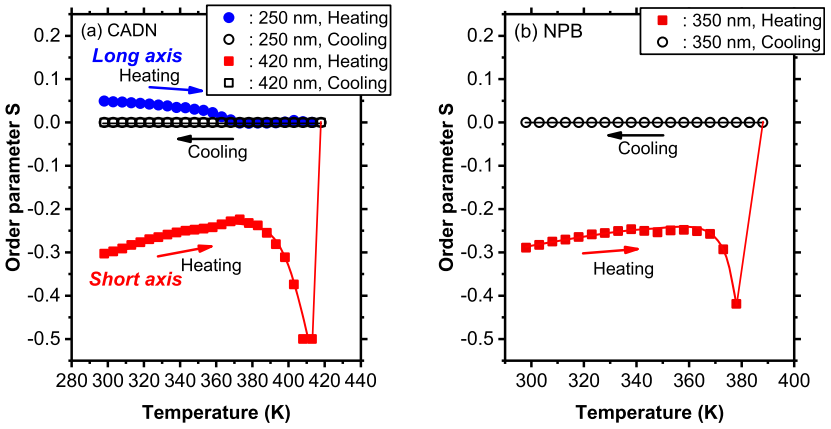

Figure 3. Dependence of the order parameter S on temperature during a single heating and cooling cycle from RT to phase transition: (a) CADN; (b) NPB. The data on the order parameter S are obtained by VASE. The solid lines are visual guides.

constants and/or thickness parameters are varied, and Ψ and Δ values are calculated with the Fresnel equations. The calculated Ψ and Δ values matching the experimental data best provide the optical constants (n, the refractive index, and k, the extinction coefficient) and the film thickness d of the samples. We carefully chose either an isotropic or an anisotropic model to fit the VASE data such that the mean-squared error (MSE) values are less than 10. This value does not have a physical meaning and is commonly accepted as a criterion, and the published data are actually within this standard. The surface potential of the films is measured using a Kelvin probe (KP020, KP Technology). SHG measurements are carried out only for the CADN sample. A 200 fs pulse train at 80 MHz from a titanium-doped sapphire laser oscillator (Vitesse, Coherent Inc.) is used as a fundamental light. The sample film deposited on a fused silica plate is set in a temperature-controlled furnace with light-transmission windows. The fundamental light beam is directed to the sample film at 45°. Since SHG is a nonlinear effect typically induced by strong light fields, a plano-convex lens (f = 100 mm) is used to focus the fundamental light on the sample. The SHG photons at 400 nm are detected by a cooled photomultiplier equipped with a digital photon-counting unit (H7421-40 with C8855-01, Hamamatsu Photonics K.K.). Glan-prism polarizers are used for the fundamental and SHG lights to examine the polarization dependence of signals. Similar to the ellipsometry measurements, the sample temperature is scanned stepwise by heating and cooling. At each temperature, the SHG intensity is recorded after stabilizing for 1 min.

RESULTS AND DISCUSSION

Figure 2a shows how the film thickness of vapor-deposited CADN at RT as the substrate temperature varies, as determined by spectroscopic ellipsometry. The molecules in the as-deposited films at RT must be packed in a well-balanced, optimized way because of the thermodynamic force that competes with the surface mobility of molecules during vapor deposition.[34] During the heating process from RT, the as-deposited film expands as a solid phase because of the activation of molecular vibrations and rotations, thereby decreasing the density of films and increasing the film thickness. At T_{onset}, which is higher than T_g, the amorphous as-deposited film begins to change phase from solid to liquid and transforms into a supercooled liquid (SCL). At this temperature, the film thickness changes abruptly and discontinuously, similar to a first phase transition. When the sample, which has entirely become an SCL, is gradually cooled at a controlled rate, the thickness linearly decreases until the temperature reaches T_g. Below T_g, the film enters another amorphous state as a glassy liquid-cooled solid phase. Since the coefficient of thermal expansion differs between the SCL and glass states, the slope of the change in film thickness with

DOI: 10.1021/acsomega.8b02560
ACS Omega 2019, 4, 39−47

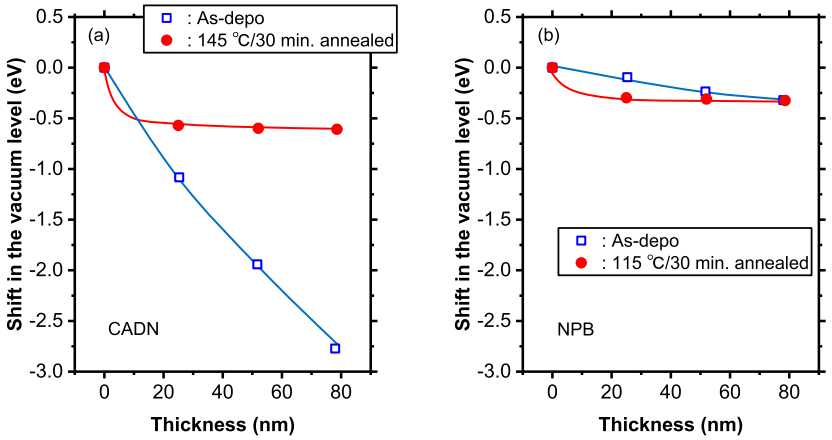

Figure 4. Shift in the vacuum level as a function of the film thickness of (a) CADN and (b) NPB. The solid lines are visual guides.

temperature is different. Performing measurements under ambient atmosphere or N_2 atmosphere does not affect these observations. As a reference, an as-deposited NPB film was also measured during the same heating and cooling cycle. The observations in Figure 2b are similar to those of previous studies,[34] thus confirming the reliability of the measurement and analysis procedures. The similarity in the behavior of the two samples suggests that CADN molecules are similar to the NPB molecules on the substrates under the temperature scanning of the as-deposited films in terms of the temperature dependence of the film thickness.

How does the molecular alignment in the as-deposited amorphous film change during a single cycle of heating and cooling from RT to the phase-transition temperature? The counterpart parameters determined together with the film thickness d by VASE are the optical constants n and k. With the obtained k, Figure 3 shows how the order parameter S of the as-deposited films changes with temperature. We carefully and consistently chose either a uniaxial or an isotropic fitting model and fit the data to deduce n and k. During heating, the anisotropic model with respect to the surface normal is inevitably needed to maintain the quality of the fit. The order parameter S is described as follows[41,42]

$$S = \frac{3}{2}\langle \cos^2 \theta \rangle - \frac{1}{2} = \frac{k_e - k_o}{k_e + 2k_o}$$

where k_e and k_o are the extinction coefficients for the surface normal and the surface plane, respectively. Using the absorption bands due to the transition dipole moments in the directions close to the long (y-axis) and short (x-axis) to the anthracene moiety of the CADN molecule, namely, 250 and 420 nm, respectively, the order parameter S for these directions in the CADN molecule can be independently obtained from the deduced k_e and k_o values at each wavelength. For the short axis of the anthracene moiety of the CADN molecule, the order parameter S at RT was determined to be S = ∼−0.3, which means that the two naphthalene moieties tend to be roughly parallel to the surface. In terms of the molecular conformation, the two naphthalene units may show the anti or syn conformations. However, they cannot be distinguished in this study because the difference between how the two conformations appear in the UV−visible spectra is not clear. However, even if the two conformations are present in the film at a certain ratio, the absorption wavelengths due to the two distinctive dipoles do not change as long as the ratio does not change. In fact, the spectra obtained from VASE are the same in terms of the absorption wavelength throughout the experiments. In Figure 3a, the absolute values of S initially decrease during heating until ∼370 K, suggesting that increasing temperature activates the vibrations and rotations of the molecules and slightly randomizes the initial alignment structure. Interestingly, however, S decreases further toward S = ∼−0.5, suggesting that the anisotropy increases as the temperature further increases until the phase transition. This means that with increasing temperature, the two naphthalene moieties of the molecules turn to align in directions parallel to the surface of the substrate. This surprising finding was determined extremely carefully to deduce the optical constants n and k with the thickness d, as described above. In the solid state of the as-deposited CADN thin films, the isotropic model gives only the nonstandard values MSE = ∼15−20, enabling us to consistently use the anisotropic model. Notably, the anisotropy, which first slightly decreases because of randomization, but increases with increasing temperature until the phase transition, can also be observed for the NPB films (Figure 3b). For both cases, the fitting quality is still good with the values of MSE = 4−7, indicating that the results are reliable.

In addition to the anthracene moiety's short axis, the order parameters S were deduced for its long axis and compared with those of its counterpart in Figure 3a. The value of S at RT was determined to be S = ∼0.05, which is almost zero. However, this does not mean that the alignment is almost isotropic; in a previous study, we revealed that the long axis of the anthracene moiety of MADN molecules,[21] which are identical to CADN except for the atomic group attached to the anthracene moiety, sit in the as-deposited thin films at the magic angle with respect to the surface normal. Presumably, the molecular orientation of the CADN molecules in this case is more or less similar to that of the MADN molecules in the previous study. During heating from RT to phase transition, the values of S decrease almost monotonically and approach S = 0. Interestingly, as further evidence of the anisotropic molecular orientation (not alignment) in the as-deposited thin films at RT, the Kelvin probe technique reveals how the vacuum level and work function change as the deposited film thickness increases (Figure 4). The vacuum level of the film with no thermal treatment gradually shifts as a function of the film thickness, whereas the film annealed over 145 °C shows a change in the vacuum level only at the interface. These results were also

DOI: 10.1021/acsomega.8b02560
ACS Omega 2019, 4, 39−47

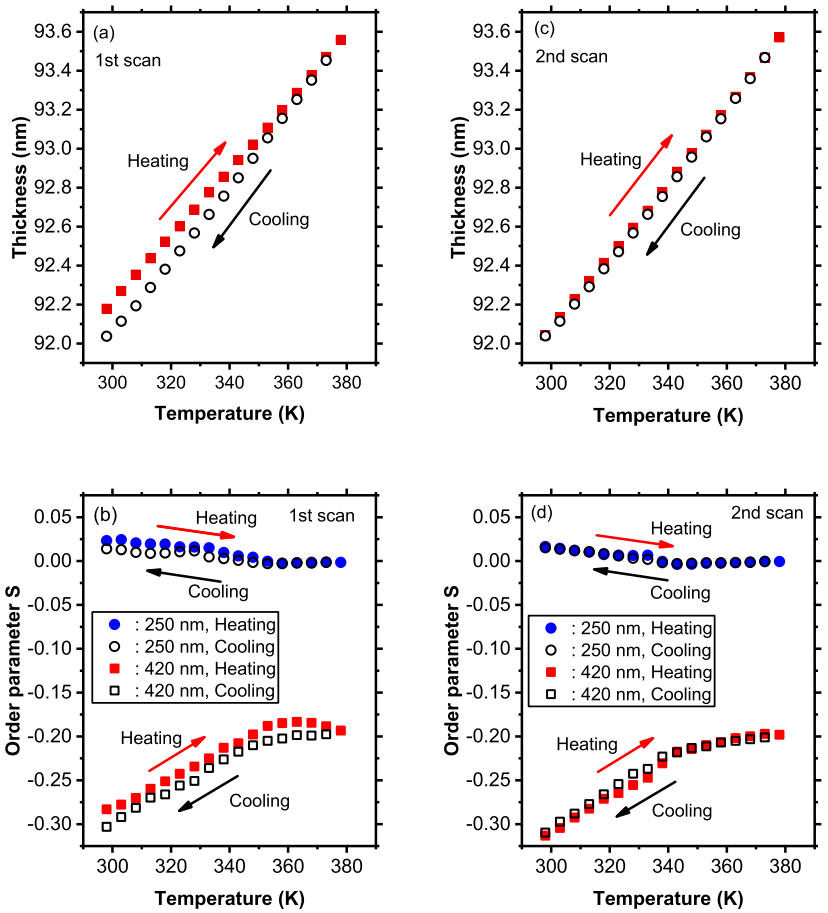

Figure 5. Temperature dependence of the film thickness (a, c) and the order parameter (b, d) of the CADN film, respectively. The temperature is varied by heating and cooling in a single cycle from RT (298 K) to 378 K. (a, b) First scan; (c, d) second scan.

previously obtained for the MADN films.[21] Comparing the results in Figure 4a,b reveals how significantly large polarizations are created in the bulk of the as-deposited CADN film. The results support the different molecular orientations (not alignment) depending on the temperature treatment of the film on substrates. The gradual change in the vacuum level observed at RT suggests that the dipoles of molecules are oriented in a certain way, and these dipoles are accumulated along the thickness direction from the surface of the substrate to the bulk of CADN; thus, a large polarization is formed in the bulk. Therefore, the orientation of the anthracene moiety is not isotropic, but anisotropic in the bulk of as-deposited films at RT.

As another notable characteristic, before the substrate temperature reaches the phase-transition temperature during heating, the anisotropy of the molecular alignment is quasi-reversible. Figure 5 shows how the anisotropy remains in the CADN films when the maximum heating temperature is below the phase transition. In the first cycle of heating and cooling, the initially observed anisotropy clearly remains with a slight variation when the films are cooled slowly back to RT; yet, it is hard to conclude that the anisotropy slightly increased or decreased after the first temperature scan. However, this variation may have been caused by the slight change in the molecular alignment at increased temperatures. During the second temperature scan, the parameters in the heating and the cooling processes are quite reproducible, suggesting that the first heating process released distorted mechanical stresses in the molecular packing and stabilized the molecular alignment.

When the phase transition begins at 418 K, T_{onset}, the isotropic model becomes appropriate, satisfying the criteria MSE < 10, which suggests that the solid-to-SCL transition indeed accompanies the disappearance of the anisotropic molecular alignment. After the phase transition for both CADN and NPB films, the isotropic model provides a good fit; therefore, all order parameters S during cooling are zero, meaning that the anthracene moieties of the CADN molecules are randomly aligned in the films. Anisotropic molecular alignment can only be observed in the amorphous solid phase of virgin as-deposited films, which have not experienced the phase transition with increasing temperature. Although the as-deposited films are heated above T_{onset} and the films experience a phase transition, anisotropic molecular alignment is no longer observed in the amorphous solid phase obtained by decreasing the temperature.

We also use SHG, a second-order nonlinear optical technique, as a complementary probing method to clarify the molecular orientations in the deposited CADN films. Since the CN group is a strong electron acceptor, the molecule itself should have a large permanent dipole moment. In such a case, SHG probes the macroscopic polar ordering of the molecules in the sample film. However, the hyperpolarizability (β) along the CN axis of the anthracene moiety is not necessarily dominant because of the two naphthalene units and the partial overlap of the absorption band of the short axis of the

DOI: 10.1021/acsomega.8b02560
ACS Omega 2019, 4, 39−47

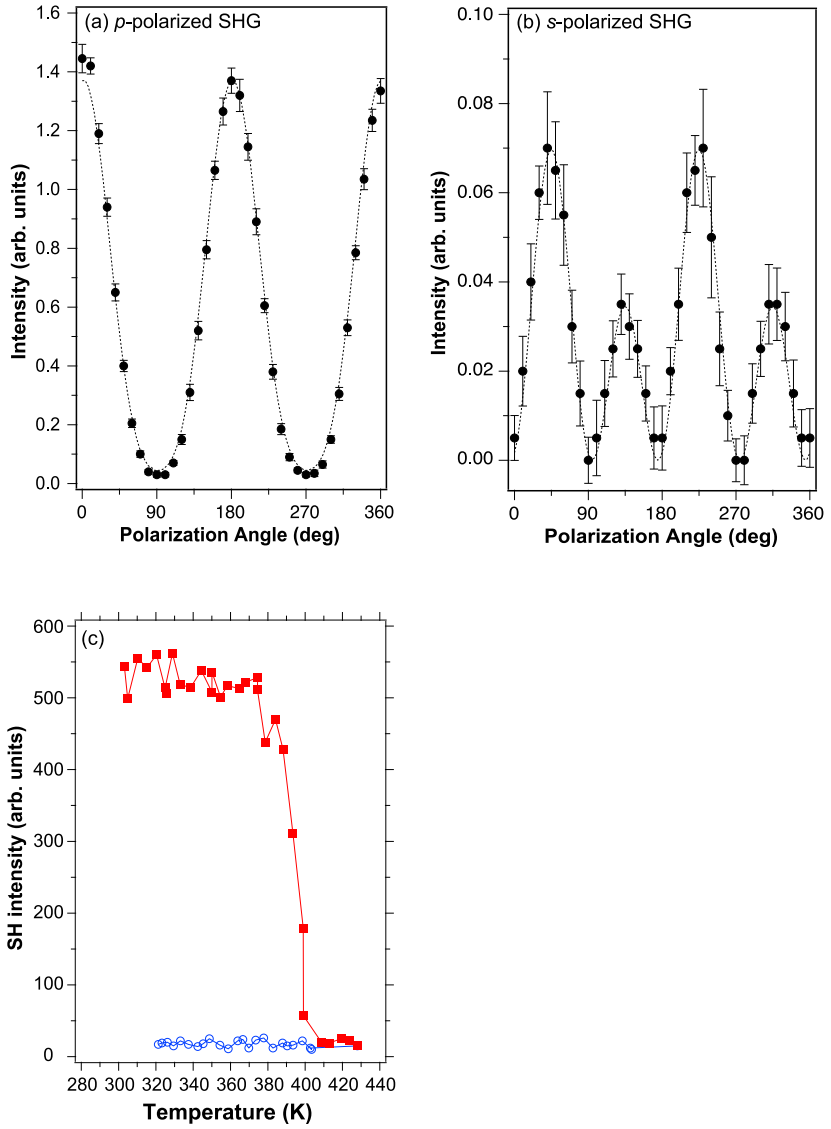

Figure 6. SHG measurements for the CADN film. (a, b) Input polarization angle dependences of (a) p-polarized and (b) s-polarized SHG signals. Error bars are given by the standard deviations. The numerical calculations (dotted curves) well fit the experimental results. (c) Temperature dependence of the SHG signals during heating (red squares) and cooling (blue open circles).

anthracene with the SHG wavelength. According to the DFT calculations at the B3LYP/6-31G(d) level, we obtain $|\beta_{\zeta\zeta\zeta}/\beta_{\eta\eta\eta}| \sim 200$ for 4-cyano-4′-penthylbiphenyl, whereas $|\beta_{\zeta\zeta\zeta}/\beta_{\eta\eta\eta}| \sim 3.4$ for CADN (Table S2), wherein the ζ-axis is set along the CN axis, with the η axis being in the plane of the two naphthalene units. β along the CN axis of the anthracene moiety is not dominant, but is the largest in the CADN molecule. Here, we do not need to use SHG to quantitatively determine the molecular orientation of CADN; the molecular orientation is already obtained by analyzing the nonlinear susceptibilities using sum-frequency generation spectroscopy, as performed in the previous study with MADN,[21] which also exhibits similar behaviors in the VASE measurements. SHG is more beneficial for the present study because it provides a simplified method to probe how the polar structure changes as a function of temperature.

In the as-deposited film, clear signals are confirmed for the p-polarized fundamental and p-polarized SHG condition, indicating polar ordering. To further verify the symmetric property, the nonlinear susceptibility tensor $\overline{\chi}$ was examined by observing how the SHG signal varies upon rotation of the input polarization. Figure 6a,b show the variation in the p- and s-polarized SHG signals as a function of the input polarization angle, defined as the relative angle between the incident plane and the polarization of the fundamental light. These experimental data can be simultaneously fitted, as shown by the broken lines in Figure 6a,b, with Fresnel factors and the film thickness ignored for simplification. The optical resonance effect, that is, imaginary contributions in $\overline{\chi}$, is also ignored. Under these assumptions, the formation of $\overline{\chi}$ was determined to be

$$\overline{\chi} = \begin{pmatrix} 0 & 0 & 0 & 0 & 0.109 & 0 \\ 0.014 & 0.014 & 0.018 & 0.127 & 0 & 0 \\ 0.107 & 0.121 & 1 & 0.018 & 0 & 0 \end{pmatrix}$$

where the Z-axis is normal to the film and the X-axis is parallel to the intersection line of the film and the light-incident planes. The values were normalized with $\chi_{ZZZ} = 1$. Clearly, SHG mainly arises from five components, χ_{ZZZ}, χ_{ZXX}, χ_{ZYY}, χ_{YYZ}, and

DOI: 10.1021/acsomega.8b02560
ACS Omega 2019, 4, 39−47

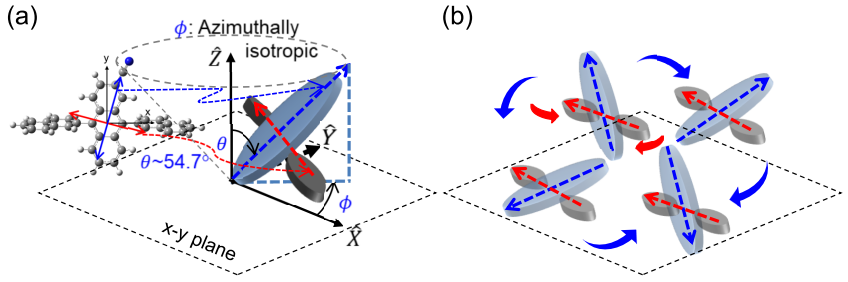

Figure 7. Schematics of (a) the molecular orientation of the CADN molecules at RT and (b) changes in their molecular orientation with increasing temperature. Blue arrows: randomization of the anthracene with respect to the polar angle. Red arrows: azimuthal rotation.

χ_{XZX}, whereas the others were almost eliminated. Actually, these five components correspond to the nonvanished ones for the $C_{\infty V}$ point group (with the ∞-fold axis parallel to the Z-axis). This result is reasonable because the present system is considered polar, but nearly isotropic in the film plane, as inferred by VASE and surface potential experiments. Notably, the so-called Kleinman's law, $\chi_{ZXX} = \chi_{XZX}$ and $\chi_{ZYY} = \chi_{YYZ}$, is satisfied, ensuring the validity of the assignment.

SHG signals should also vary with temperature. Figure 6c shows the SHG signals for p-polarized fundamental and p-polarized SHG lights monitored while heating and cooling the sample film. Upon heating to about 370 K, the initial signal slightly decreases, clearly corresponding to the behavior of S (Figure 3a), that is, increasing temperature activates molecular motion and randomizes the initial molecular orientations. Then, the signal significantly drops toward T_g, above which the signal is almost negligible. The SHG signals of the long axis of the anthracene moiety decrease with increasing temperature because of randomization, while the axis of the two naphthalene moieties becomes flatter on the surface with azimuthal isotropy, which also reduces the SHG signals. Thus, the molecular orientations are fully randomized by the phase transition, after which the polar ordering never recovers, even by cooling to almost RT.

Figure 7 schematically illustrates the molecular orientations of the CADN molecules in the films at RT and their approximate changes with increasing temperature. Based on the previous study using sum-frequency generation spectroscopy on MADN and the VASE observations of CADN, which are similar to those of MADN,[21] the molecular orientation of the CADN molecules can be depicted as in Figure 7a. The short axis of the anthracene moiety slightly tilts from the surface plane, but preferentially stays close to the surface with a certain orientational distribution. Meanwhile, on average, the long axis of the anthracene moiety is oriented close to the magic angle from the surface normal.

Interestingly, randomization and constraint of the molecular alignment and orientation are observed to coexist in the CADN molecule as the temperature increases toward the phase transition. Specifically, the long axis of the anthracene moiety is randomized, becoming isotropic from the previously anisotropic orientation at the magic angle, whereas the short axis of the anthracene, which is the long axis along the two naphthalene moieties, shows the opposite behavior, i.e., increasing anisotropy of the molecular alignment. These molecular alignments and orientations are possible because the polar angle with respect to the surface normal is the only influencing factor, and the system is azimuthally isotropic with free twist rotations around the axes. Figure 7b illustrates such changes in the molecular orientation of a CADN molecule with increasing temperature, especially close to the phase-transition temperature. Note that these molecular orientations are not at the surface but in the bulk. The long axis of the anthracene moiety can be randomized with respect to the polar angle, whereas the axis of the two naphthalene moieties remains almost parallel to the surface plane of the substrate. The blue arrows indicate the changes in the molecular motion of the anthracene moiety. The axis of the two naphthalene units can remain in the surface plane regardless of the tilting of the anthracene moiety with respect to the polar angle. Surprisingly, the axis of the two naphthalene units becomes flatter on the surface, demonstrating this restricted behavior. The entire molecules are azimuthally isotropic. In Figure 7b, the red arrows indicate the possible azimuthal rotations. The randomized and constrained parts of the molecules may compensate the total entropy of the whole molecular system.

Since the CADN molecule has two moieties, the alignment and orientation of which can be simultaneously probed, we observe almost the opposite behaviors: the randomization and constraint of both molecular alignment and orientation in the molecule. However, this is not observed with other typical OSC molecules. We probe the degree of molecular motions through the order parameters of the molecules using VASE. The similarity between the trends of the CADN and NPB molecules arises from their similar behaviors, i.e., that their molecular motions become active and randomized with increasing temperature. However, our study suggests that not all parts of a molecule can necessarily be randomized uniformly as the temperature increases. One moiety of a molecule becomes randomized with increasing temperature, but another moiety exhibits the opposite behavior near the phase-transition temperature. This is the case with CADN in this study, which is presumably similar to MADN. However, NPB may also exhibit the same feature. The only difference between CADN and NPB is the number of axes (moieties) of the molecule that can be probed using VASE. We can independently probe the two distinctive moieties in the case of CADN, but we can monitor only one axis of the molecule in the case of NPB. Nonetheless, we may be able to extend these observations to other molecular systems, including NPB. Not all parts of a molecule would be necessarily randomized in the same way in terms of the molecular alignment and orientation with increasing temperature; one part of the moiety may be randomized, whereas another part of the moiety may be restricted and constrained as the temperature approaches the phase-transition temperature.

CONCLUSIONS

In summary, randomization and constraint are found to coexist in the CADN molecular alignment and orientation. Using

DOI: 10.1021/acsomega.8b02560
ACS Omega 2019, 4, 39−47

VASE and SHG, we observed changes in the molecular alignment and orientation of CADN molecules in vapor-deposited films by heating and cooling the samples in a cycle from RT to the phase-transition temperature. In the as-deposited amorphous films at RT, the anisotropic alignment of the short axis of the anthracene moiety, that is, the naphthalene moiety, is roughly parallel to the surface of the substrates, whereas the long axis of the anthracene moiety is closely oriented by the magic angle with respect to the surface normal. Although the anisotropic alignment of the naphthalene moiety initially decreases during heating, the anisotropy notably increases as the temperature approaches the film's phase-transition temperature. The anthracene moiety's long axis significantly changes as the anisotropic orientation decreases monotonically with respect to the surface normal from the magic angle to isotropy. The initial order parameter S of the long axis of the anthracene moiety is almost zero; however, it is not isotropic, but anisotropic, and the orientation is almost the magic angle, as verified by SHG signals. As the film temperature increases, the SHG signals weaken monotonically, and eventually, no SHG signals are observed, corresponding to the isotropic orientation. The isotropic orientation of the anthracene moiety's long axis below the phase-transition temperature is also notable, with the axis of the two naphthalene units being more constrained and flat on the surface plane. After heating above this temperature, all molecular orientations are isotropic. Probing the anisotropy of the CADN molecule's two moieties potentially reveals that the molecular alignment and orientation undergo a two-step transformation through the coexistence of randomization and constraint of parts of the molecule as the temperature varies near the phase-transition temperature.

■ ASSOCIATED CONTENT

Supporting Information

The Supporting Information is available free of charge on the ACS Publications website at DOI: 10.1021/acsomega.8b02560.

DFT calculations on the ground-to-excited-state transition dipole moments and hyperpolarizability tensor components (PDF)

■ AUTHOR INFORMATION

Corresponding Author

*E-mail: oh-e@ee.nthu.edu.tw

ORCID

Masahito Oh-e: 0000-0003-3411-4340

Notes

The authors declare no competing financial interest.

■ ACKNOWLEDGMENTS

This work was supported by a grant from Nissan Chemical Co. (NTHU no. 17093068) through an industrial-academic collaboration project.

■ REFERENCES

(1) Lin, H.-W.; Lin, C.-L.; Chang, H.-H.; Lin, Y.-T.; Wu, C.-C.; Chen, Y.-M.; Chen, R.-T.; Chien, Y.-Y.; Wong, K.-T. Anisotropic Optical Properties and Molecular Orientation in Vacuum-Deposited Ter(9,9-Diarylfluorene)s Thin Films Using Spectroscopic Ellipsometry. *J. Appl. Phys.* **2004**, *95*, 881−886.

(2) Yokoyama, D.; Sakaguchi, A.; Suzuki, M.; Adachi, C. Horizontal Molecular Orientation in Vacuum-Deposited Organic Amorphous Films of Hole and Electron Transport Materials. *Appl. Phys. Lett.* **2008**, *93*, No. 173302.

(3) Yokoyama, D.; Sakaguchi, A.; Suzuki, M.; Adachi, C. Horizontal Orientation of Linear-Shaped Organic Molecules Having Bulky Substituents in Neat and Doped Vacuum-Deposited Amorphous Films. *Org. Electron.* **2009**, *10*, 127−137.

(4) Yokoyama, D.; Setoguchi, Y.; Sakaguchi, A.; Suzuki, M.; Adachi, C. Orientation Control of Linear-Shaped Molecules in Vacuum-Deposited Organic Amorphous Films and Its Effect on Carrier Mobilities. *Adv. Funct. Mater.* **2010**, *20*, 386−391.

(5) Frischeisen, J.; Yokoyama, D.; Endo, A.; Adachi, C.; Brütting, W. Increased Light Outcoupling Efficiency in Dye-Doped Small Molecule Organic Light-Emitting Diodes with Horizontally Oriented Emitters. *Org. Electron.* **2011**, *12*, 809−817.

(6) Yokoyama, D.; Adachi, C.; Kinoshita, T.; Maruyama, E.; Tanaka, M.; Shirakawa, M.; Shibata, K.; Woollam, J. A.; Ziener, U.; Chang, C.; et al. Molecular Orientation in Small-Molecule Organic Light-Emitting Diodes. *J. Mater. Chem.* **2011**, *21*, 19187.

(7) Tumbleston, J. R.; Collins, B. A.; Yang, L.; Stuart, A. C.; Gann, E.; Ma, W.; You, W.; Ade, H. The Influence of Molecular Orientation on Organic Bulk Heterojunction Solar Cells. *Nat. Photonics* **2014**, *8*, 385−391.

(8) Marchetti, A. P.; Haskins, T. L.; Young, R. H.; Rothberg, L. J. Permanent Polarization and Charge Distribution in Organic Light-Emitting Diodes (OLEDs): Insights from near-Infrared Charge-Modulation Spectroscopy of an Operating OLED. *J. Appl. Phys.* **2014**, *115*, No. 114506.

(9) Wakamiya, A.; Nishimura, H.; Fukushima, T.; Suzuki, F.; Saeki, A.; Seki, S.; Osaka, I.; Sasamori, T.; Murata, M.; Murata, Y.; et al. On-Top π-Stacking of Quasiplanar Molecules in Hole-Transporting Materials: Inducing Anisotropic Carrier Mobility in Amorphous Films. *Angew. Chem., Int. Ed.* **2014**, *53*, 5800−5804.

(10) Shibata, M.; Sakai, Y.; Yokoyama, D. Advantages and Disadvantages of Vacuum-Deposited and Spin-Coated Amorphous Organic Semiconductor Films for Organic Light-Emitting Diodes. *J. Mater. Chem. C* **2015**, *3*, 11178−11191.

(11) Tang, C. W.; VanSlyke, S. A. Organic Electroluminescent Diodes. *Appl. Phys. Lett.* **1987**, *51*, 913−915.

(12) Nelson, J. Polymer:Fullerene Bulk Heterojunction Solar Cells. *Mater. Today* **2011**, *14*, 462−470.

(13) Koezuka, H.; Tsumura, A.; Ando, T. Field-Effect Transistor with Polythiophene Thin Film. *Synth. Met.* **1987**, *18*, 699−704.

(14) Mayr, C.; Taneda, M.; Adachi, C.; Brütting, W. Different Orientation of the Transition Dipole Moments of Two Similar Pt(II) Complexes and Their Potential for High Efficiency Organic Light-Emitting Diodes. *Org. Electron.* **2014**, *15*, 3031−3037.

(15) Komino, T.; Tanaka, H.; Adachi, C. Selectively Controlled Orientational Order in Linear-Shaped Thermally Activated Delayed Fluorescent Dopants. *Chem. Mater.* **2014**, *26*, 3665−3671.

(16) Kearns, K. L.; Na, H.-Y.; Froese, R. D.; Mukhopadhyay, S.; Woodward, H.; Welsh, D.; DeVries, T.; Devore, D.; Trefonas, P.; Hong, L. *Molecular Orientation, Thermal Behavior and Density of Electron and Hole Transport Layers and the Implication on Device Performance for OLEDs*, Proc. SPIE 9183, Organic Light Emitting Materials and Devices XVIII; So, F., Adachi, C., Eds.; 2014; pp 91830F-1−91830F-12.

(17) Yokoyama, D.; Sasabe, H.; Furukawa, Y.; Adachi, C.; Kido, J. Molecular Stacking Induced by Intermolecular C-H···N Hydrogen Bonds Leading to High Carrier Mobility in Vacuum-Deposited Organic Films. *Adv. Funct. Mater.* **2011**, *21*, 1375−1382.

(18) Chen, W.-C.; Yuan, Y.; Wu, G.-F.; Wei, H.-X.; Tang, L.; Tong, Q.-X.; Wong, F.-L.; Lee, C.-S. Staggered Face-to-Face Molecular Stacking as a Strategy for Designing Deep-Blue Electroluminescent Materials with High Carrier Mobility. *Adv. Opt. Mater.* **2014**, *2*, 626−631.

(19) Hiszpanski, A. M.; Loo, Y.-L.; Briseno, A. L.; Crosby, A. J.; Yu, S.; Hou, Y.; Zou, B.; Cui, T.; Zou, G.; Sundqvist, B.; et al. Directing

DOI: 10.1021/acsomega.8b02560
ACS Omega 2019, 4, 39−47

the Film Structure of Organic Semiconductors via Post-Deposition Processing for Transistor and Solar Cell Applications. *Energy Environ. Sci.* **2014**, *7*, 592−608.
(20) Dale, R. E.; Eisinger, J.; Blumberg, W. E. The Orientational Freedom of Molecular Probes. The Orientation Factor in Intramolecular Energy Transfer. *Biophys. J.* **1979**, *26*, 161−193.
(21) Oh-e, M.; Ogata, H.; Fujita, Y.; Koden, M. Anisotropy in Amorphous Films of Cross-Shaped Molecules with an Accompanying Effect on Carrier Mobility: Ellipsometric and Sum-Frequency Vibrational Spectroscopic Studies. *Appl. Phys. Lett.* **2013**, *102*, No. 101905.
(22) Frischeisen, J.; Yokoyama, D.; Adachi, C.; Brütting, W. Determination of Molecular Dipole Orientation in Doped Fluorescent Organic Thin Films by Photoluminescence Measurements. *Appl. Phys. Lett.* **2010**, *96*, No. 073302.
(23) Kuma, H.; Hosokawa, C. Blue Fluorescent OLED Materials and Their Application for High-Performance Devices. *Sci. Technol. Adv. Mater.* **2014**, *15*, No. 034201.
(24) Ogiwara, T.; Ito, H.; Mizuki, Y.; Naraoka, R.; Funahashi, M.; Kuma, H. Efficiency Improvement of Fluorescent Blue Device by Molecular Orientation of Blue Dopant. *J. Soc. Inf. Disp.* **2014**, *22*, 76−82.
(25) Kim, B.; Park, Y.; Lee, J.; Yokoyama, D.; Lee, J.-H.; Kido, J.; Park, J.; Kim, T. H.; Kim, K. S.; Park, J.; et al. Synthesis and Electroluminescence Properties of Highly Efficient Blue Fluorescence Emitters Using Dual Core Chromophores. *J. Mater. Chem. C* **2013**, *1*, 432−440.
(26) Marcus, R. A. Electron Transfer Reactions in Chemistry. Theory and Experiment. *Rev. Mod. Phys.* **1993**, *65*, 599−610.
(27) Yamada, T.; Sato, T.; Tanaka, K.; Kaji, H. Percolation Paths for Charge Transports in N,N′-Diphenyl-N,N′-Di(m-Tolyl)Benzidine (TPD). *Org. Electron.* **2010**, *11*, 255−265.
(28) Evans, D. R.; Kwak, H. S.; Giesen, D. J.; Goldberg, A.; Halls, M. D.; Oh-e, M. Estimation of Charge Carrier Mobility in Amorphous Organic Materials Using Percolation Corrected Random-Walk Model. *Org. Electron.* **2016**, *29*, 50−56.
(29) Swallen, S. F.; Kearns, K. L.; Mapes, M. K.; Kim, Y. S.; McMahon, R. J.; Ediger, M. D.; Wu, T.; Yu, L.; Satija, S. Organic Glasses with Thermodynamic and Kinetic Stability. *Science* **2007**, *315*, 353−357.
(30) Leon-Gutierrez, E.; Garcia, G.; Lopeandia, A. F.; Clavaguera-Mora, M. T.; Rodríguez-Viejo, J. Size Effects and Extraordinary Stability of Ultrathin Vapor Deposited Glassy Films of Toluene. *J. Phys. Chem. Lett.* **2010**, *1*, 341−345.
(31) Zhu, L.; Brian, C. W.; Swallen, S. F.; Straus, P. T.; Ediger, M. D.; Yu, L. Surface Self-Diffusion of an Organic Glass. *Phys. Rev. Lett.* **2011**, *106*, No. 256103.
(32) Ahrenberg, M.; Chua, Y. Z.; Whitaker, K. R.; Huth, H.; Ediger, M. D.; Schick, C. *In Situ* Investigation of Vapor-Deposited Glasses of Toluene and Ethylbenzene via Alternating Current Chip-Nanocalorimetry. *J. Chem. Phys.* **2013**, *138*, No. 024501.
(33) Dalal, S. S.; Fakhraai, Z.; Ediger, M. D. High-Throughput Ellipsometric Characterization of Vapor-Deposited Indomethacin Glasses. *J. Phys. Chem. B* **2013**, *117*, 15415−15425.
(34) Dalal, S. S.; Walters, D. M.; Lyubimov, I.; dePablo, J. J.; Ediger, M. D. Tunable Molecular Orientation and Elevated Thermal Stability of Vapor-Deposited Organic Semiconductors. *Proc. Natl. Acad. Sci. U.S.A.* **2015**, *112*, 4227−4232.
(35) Woollam, J. A.; Johs, B. D.; Herzinger, C. M.; Hilfiker, J. N.; Synowicki, R. A.; Bungay, C. L. In *Overview of Variable-Angle Spectroscopic Ellipsometry (VASE): I. Basic Theory and Typical Applications*, SPIE CR72, 1999; p 3.
(36) Fujiwara, H. *Spectroscopic Ellipsometry*; John Wiley & Sons, Ltd: Chichester, U.K., 2007.
(37) Shen, Y. R. *The Principles of Nonlinear Optics*; Wiley-Interscience: New York, 1984.
(38) Frisch, M. J.; Trucks, G. W.; Schlegel, H. B.; Scuseria, G. E.; Robb, M. A.; Cheeseman, J. R.; Scalmani, G.; Barone, V.; Mennucci, B.; Petersson, G. A.; Nakatsuji, H.; Caricato, M.; Li, X.; Hratchian, H. P.; Izmaylov, A. F.; Bloino, J.; Zheng, G.; Sonnenberg, J. L.; Hada, M.; Ehara, M.; Toyota, K.; Fukuda, R.; Hasegawa, J.; Ishida, M.; Nakajima, T.; Honda, Y.; Kitao, O.; Nakai, H.; Vreven, T.; Montgomery, J. A., Jr.; Peralta, J. E.; Ogliaro, F.; Bearpark, M.; Heyd, J. J.; Brothers, E.; Kudin, K. N.; Staroverov, V. N.; Kobayashi, R.; Normand, J.; Raghavachari, K.; Rendell, A.; Burant, J. C.; Iyengar, S. S.; Tomasi, J.; Cossi, M.; Rega, N.; Millam, J. M.; Klene, M.; Knox, J. E.; Cross, J. B.; Bakken, V.; Adamo, C.; Jaramillo, J.; Gomperts, R.; Stratmann, R. E.; Yazyev, O.; Austin, A. J.; Cammi, R.; Pomelli, C.; Ochterski, J. W.; Martin, R. L.; Morokuma, K.; Zakrzewski, V. G.; Voth, G. A.; Salvador, P.; Dannenberg, J. J.; Dapprich, S.; Daniels, A. D.; Farkas, Ö.; Foresman, J. B.; Ortiz, J. V.; Cioslowski, J.; Fox, D. J. *Gaussian 09*, revision B.01; Gaussian, Inc.: Wallingford, CT, 2009.
(39) van Mensfoort, S. L. M.; Shabro, V.; deVries, R. J.; Janssen, R. A. J.; Coehoorn, R. Hole Transport in the Organic Small Molecule Material α-NPD: Evidence for the Presence of Correlated Disorder. *J. Appl. Phys.* **2010**, *107*, No. 113710.
(40) Torres, J. M.; Bakken, N.; Li, J.; Vogt, B. D. Substrate Temperature to Control Moduli and Water Uptake in Thin Films of Vapor Deposited N,N′-Di(1-Naphthyl)-N,N′-Diphenyl-(1,1′-Biphenyl)-4,4′-Diamine (NPD). *J. Phys. Chem. B* **2015**, *119*, 11928−11934.
(41) Bernstein, R. B.; Choit, S. E.; Stolte, S. Determination of Molecular Orientation and Alignment from Polarized Laser Photofragmentation Measurements Oriented CH3 I Molecular Beams. *J. Chem. Soc., Faraday Trans. 2* **1989**, 1097.
(42) Dunmur, D.; Toriyama, K. Optical Properties. In *Physical Properties of Liquid Crystals*; Demus, D., Goodby, J., Gray, G. W., Spiess, H.-W., Vill, V., Eds.; Wiley-VCH: Weinheim, 1999; pp 113−128.

DOI: 10.1021/acsomega.8b02560
ACS Omega 2019, 4, 39−47